Molecular Therapy
Original Article

Therapeutic Genome Editing for Myotonic Dystrophy Type 1 Using CRISPR/Cas9

Yanlin Wang,[1,11] Lei Hao,[2,11] Hongcai Wang,[3,4] Katherine Santostefano,[5] Arjun Thapa,[4] John Cleary,[6] Hui Li,[7] Xiuming Guo,[8] Naohiro Terada,[5] Tetsuo Ashizawa,[9] and Guangbin Xia[4,10]

[1]Department of Neurology, The First Affiliated Hospital of Zhengzhou University, Henan 450000, China; [2]Department of Neurology, The Fifth People's Hospital of Chongqing, Chongqing 400062, China; [3]Department of Neurology, Affiliated Hospital of Binzhou Medical University, Binzhou City, Shandong Province, China; [4]Department of Neurology, University of New Mexico, Albuquerque, NM, USA; [5]Department of Pathology, Immunology & Laboratory Medicine, College of Medicine, University of Florida, Gainesville, FL, USA; [6]Department of Molecular Genetics and Microbiology, University of Florida, Gainesville, FL, USA; [7]Department of Neurology, University of Wisconsin, Madison, WI, USA; [8]Department of Neurology, The First Affiliated Hospital of Chongqing Medical University, Chongqing 400016, China; [9]Houston Methodist Neurological Institute and Research Institute, 6670 Bertner Ave. R11-117, Houston, TX, USA; [10]Department of Neuroscience, University of New Mexico, Albuquerque, NM, USA

Myotonic dystrophy type 1 (DM1) is caused by a CTG nucleotide repeat expansion within the 3′ UTR of the Dystrophia Myotonica protein kinase gene. In this study, we explored therapeutic genome editing using CRISPR/Cas9 via targeted deletion of expanded CTG repeats and targeted insertion of polyadenylation signals in the 3′ UTR upstream of the CTG repeats to eliminate toxic RNA CUG repeats. We found paired SpCas9 or SaCas9 guide RNA induced deletion of expanded CTG repeats. However, this approach incurred frequent inversion in both the mutant and normal alleles. In contrast, the insertion of polyadenylation signals in the 3′ UTR upstream of the CTG repeats eliminated toxic RNA CUG repeats, which led to phenotype reversal in differentiated neural stem cells, forebrain neurons, cardiomyocytes, and skeletal muscle myofibers. We concluded that targeted insertion of polyadenylation signals in the 3′ UTR is a viable approach to develop therapeutic genome editing for DM1.

INTRODUCTION

Microsatellite nucleotide repeat expansion causes many neurodegenerative disorders, including those in coding and non-coding regions (see recent reviews[1,2]). With the advancement of therapeutic genome editing (see reviews[3–8]), there is increasing enthusiasm for use of these technologies to develop therapeutics for these disorders. For nucleotide repeats in non-coding regions, there are more options for editing because there is diminished concern for the incorporation of missense or nonsense mutations during genome manipulation. Targeted contraction of the expanded CAG repeats has been performed using zinc-finger nucleases,[9] but the relatively high degree of off-target effects limits their therapeutic potential. Deletion of the nucleotide repeats using pairs of endonucleases flanking the expanded region is a promising strategy. This has been tested in a recent study on myotonic dystrophy (Dystrophia Myotonica [DM]) type 1 (DM1),[10,11] which is caused by a CTG nucleotide repeat expansion within the 3′ UTR) of the Dystrophia Myotonica protein kinase (*DMPK*) gene.[12] The expanded CTG repeats encode expanded RNA CUG repeats, which causes disease largely through RNA gain of function.[13–17]

However, targeted deletion is not without problems. It has been reported that two double-strand breaks that flank a genomic loci created by CRSPR/Cas9 result in an inversion rate between 2.2% and 6.7%. The rate was sufficient to correct a chromosomal inversion in hemophilia A.[18] Nevertheless, the study did not report the rate of targeted deletion. The ratio of targeted deletion and inversion is thus unknown. Even in the recently published paper on DM1, the authors noticed inversion of the normal allele containing 13 CTG repeats. However, inversion of the expanded allele was not studied,[10] which is more important in terms of its possible deleterious biological effects. In the current study, we tested the relative efficiency of deletion and inversion of the expanded CTG repeats by pairs of CRISPR/Cas9 guide RNAs (gRNAs) to explore whether targeted deletion could be a therapeutic option for DM1.

We have recently developed a strategy that eliminated expanded RNA CUG repeats via precise insertion of polyadenylation (PolyA) signals upstream of *DMPK* CTG repeats. The PolyA signals prematurely terminated transcription upstream of the CTG repeats. Importantly, genome-modified human DM1 induced pluripotent stem cells (iPSCs) maintain their pluripotency. DM1 iPSCs, as well as their neural and cardiomyocyte derivatives, lost intranuclear RNA CUG repeat foci and demonstrated reversal of aberrant splicing.[19,20] However, our earlier studies adopted Transcription Activator-like Effector Nuclease (TALEN) technology, which cannot target the 3′ UTR because of nucleotide hypermethylation. Therefore, we had to target intron 9

Received 7 March 2018; accepted 6 September 2018;
https://doi.org/10.1016/j.ymthe.2018.09.003.

[11]These authors contributed equally to this work.

Correspondence: Guangbin Xia, MD, PhD, Department of Neurology and Neuroscience, School of Medicine, University of New Mexico, Albuquerque, NM, USA.
E-mail: guangbin.xia@gmail.com

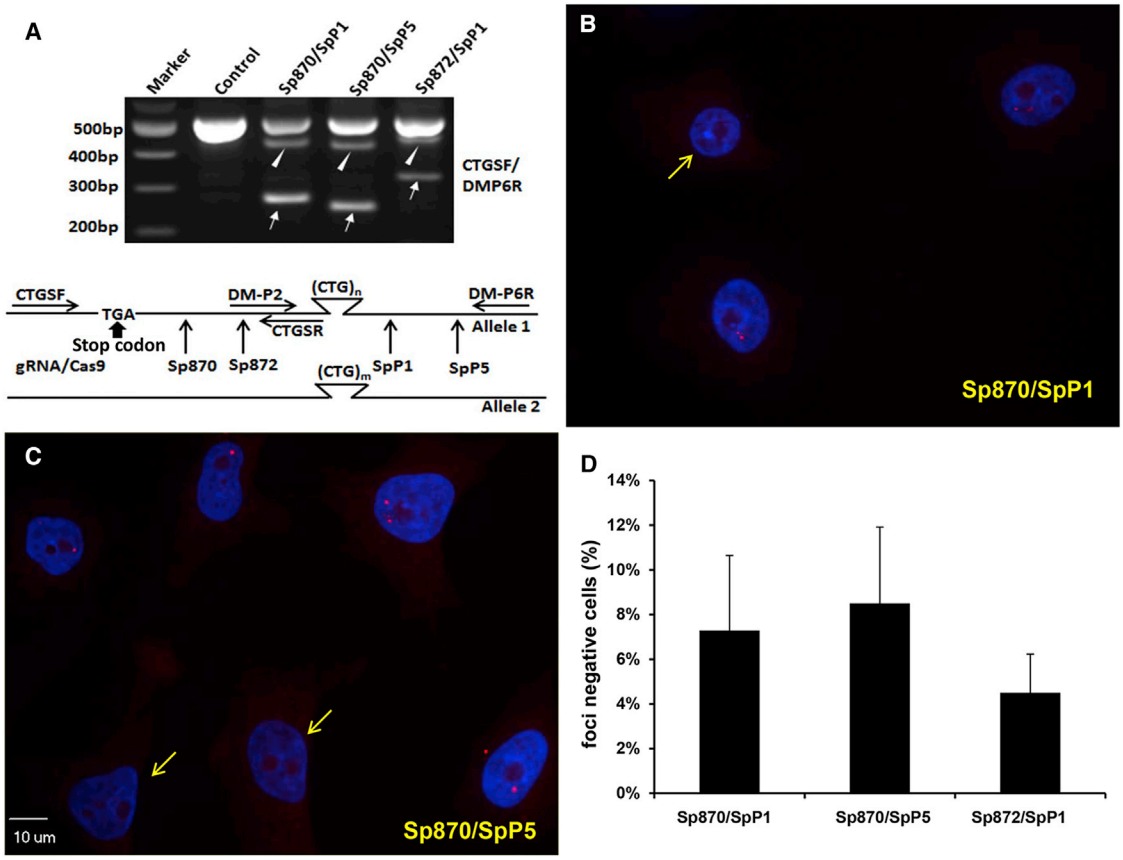

Figure 1. Targeted Deletion of the CTG Repeats by Paired SpCas9 gRNAs Flanking the CTG Repeats

(A) Targeted deletion of the CTG repeats in HEK293 FT cells. Genomic PCR using primer pair (CTGSF/DM1-P6R) that flanks the cut sites was performed using template DNA extracted from sorted HEK293 FT cells after transfection with paired SpCas9 gRNA-containing plasmids. The lower PCR products (arrows) were sequenced and confirmed to have the deletion of the flanked segment (see also Figure S1E). The middle PCR products (arrowheads) were confirmed to result from non-homologous end joining with deletion of short nucleotides after double-strand break caused by single SpCas9 gRNAs (sequencing data not shown). Primer location was indicated below the gel image. (B–D) Targeted deletion of expanded CTG repeats evaluated by the loss of intranuclear RNA CUG repeat foci in DM1 NSCs. DM1 NSCs derived from DM-03 iPSCs were transfected with paired SpCas9 gRNA plasmids and sorted 48 hr later. Cells were then plated into chamber slide and switched to DMEM supplemented with 2% horse serum for 72 hr prior to FISH. 100 cells of each of the three fields were observed, and the percentage of foci-negative cells (arrows), which reflects the deletion of the expanded repeats, were calculated and averaged. Data are represented as mean ± SEM.

for the insertion of PolyA signals to prove the feasibility of this approach. In this study, we have modified our methods by adopting CRISPR/Cas9 to insert PolyA signals in the 3′ UTR upstream of the expanded CTG repeats, which will generate an engineered *DMPK* without CUG repeats and without causing truncated DMPK protein. We found that this approach eliminated toxic RNA CUG repeats and phenotype reversal of DM1 iPSCs and their derivatives, including skeletal muscle myofibers. We conclude that this approach is a viable option for therapeutic genome editing in DM1.

RESULTS

Targeted Deletion of the CTG Repeats by Paired SpCas9 gRNAs or SaCas9 gRNAs Flanking the Expanded CTG Repeats

To delete expanded CTG repeats, we screened *Streptococcus pyogenes* Cas9 (SpCas9) gRNAs and *Staphylococcus aureus* Cas9 (SaCas9) gRNAs within 220 bp up- and downstream of the CTG repeats. We found two SpCas9 gRNAs (Sp870 and Sp872) and three SaCas9 gRNAs (Sa870U, Sa870D, and Sa872) target loci upstream of the CTG repeats, as well as two SpCas9 gRNAs (SpP1 and SpP5) and two SaCas9 gRNAs (SaP2 and SaP3) target loci downstream of the CTG repeats, creating efficient double-strand breaks when introduced individually (Figures S1A–S1D).

We then conducted an initial test in HEK293 FT cells to determine which SpCas9 gRNA pairs could efficiently induce efficient CTG repeat deletion. We found that all selected gRNA pairs flanking the CTG repeats caused deletion of the CTG repeats (Figure 1A). Sanger sequencing revealed the ends were seamlessly annealed (Figure S1E).

However, current PCR strategies using primers flanking the CTG repeats are insufficient to determine whether the deletion of CTG repeats occurs in the normal allele or mutant allele. Alternative PCR

strategies with the use of primers within the excised area are possible to demonstrate gene-editing effects on one or both DMPK alleles. However, to observe the consequence of the deletion of the expanded allele, we tested deletion efficiency by a fluorescence *in situ* hybridization (FISH) strategy in DM1 neural stem cells (NSCs) derived from a DM1 iPSC line (DM-03).[20,21] Southern blot showed that the CTG repeats further expanded in these NSCs compared to those in their parental iPSCs (Figure S2). The deletion efficiency was evaluated by measuring the percentage of cells that had lost intranuclear RNA CUG repeat foci from the population of cells that were sorted for the presence of orange fluorescent protein (OFP). OFP^+ cells were cultured for 72 hr in DMEM supplemented with 2% horse serum prior to RNA FISH. This treatment ensured that 100% of untreated DM1 NSCs contained intranuclear RNA CUG repeat foci, as we reported previously.[22] We found the deletion efficiency was generally less than 10% (Figures 1B–1D).

Since the deletion efficiency using paired SpCas9 gRNAs was relatively low, we tested whether paired SaCas9 gRNAs could induce higher deletion efficiency. One other advantage of SaCas9 is that it is shorter than SpCas9 and can be packaged into adeno-associated virus (AAV) for future *in vivo* applications. Pairwise deletion was first tested in HEK293 FT cells. We found that each pair induced targeted deletion and the ends were seamlessly annealed (Figure 2A). The deletion efficiency of the expanded CTG repeats was again tested in DM1 NSCs. NSCs were sorted for GFP-positive cells, and the deletion efficiency was evaluated by measuring the percentage of cells that lost intranuclear RNA CUG repeat foci. We found the efficiency reached as high as 52.7% using the Sa872/SaP3 pair, and some foci-negative cells were observed in clusters adjacent to foci-positive cells (Figures 2D and 2F). There is a concern that spontaneous contraction of CTG repeats in these NSCs produced the reduction of CUG repeat RNA foci. We ran FISH on the DM1 NSCs that were not subjected to SpCas9 or SaCas9 gRNAs, and we found that 100% of the NSCs were positive for RNA foci (Figure 2B) (see also Figures S3C and S5D).

Frequent Inversion of Expanded CTG Repeats by Paired gRNA-CRISPR/SaCas9

To test whether this strategy led to inversion of the sequence flanked by the gRNA pairs, we repeated the above experiment with paired SaCas9 gRNAs in DM1 NSCs, but cells were sorted to select for higher GFP expression. Again, we found an appropriate efficiency of targeted deletion (Figure 3A). However, a pair of primers that were both in the same direction (CTGSR/DM-P6R, positions are shown in Figure 2C) in the DMPK gene unexpectedly generated PCR products in the NSCs that were transfected with SaCas9 gRNA pairs (Figure 3B). We sequenced the new PCR products and confirmed the inversions at the junctional sites (Figure 3C).

To test whether this strategy led to the inversion of expanded CTG repeats, we focused the study on the Sa872/SaP3 gRNA pair in DM1 NSCs. Again, this pair produced targeted deletion and inversion by genomic PCR analysis (Figure S3A). FISH revealed the deletion of expanded CTG repeats (the percentage of foci-negative cells), the efficiency of which was positively correlated with the higher expression levels of SaCas9-GFP (Figure S3B). We then performed double FISH analysis with sense and antisense oligo probes in DM1 NSCs transfected with Sa872/SaP3. We could see that there were mixed cells, some with red foci detected by the sense oligo probes labeled with Cy3, some cells with no intranuclear RNA CUG repeat foci, and some cells with green RNA CAG repeat foci detected by the Alexa 488 antisense oligo probes. Foci labeled with the sense or antisense probes were not observed within the same cell (Figure 3D; Figures S3D–S3F). Furthermore, no antisense intranuclear RNA CAG foci were detected in untreated DM1 NSCs (Figure S3C). These findings suggested that the expanded CTG repeats were inverted in a subset of cells and became expanded CAG repeats that encoded expanded CAG RNAs, which were stable and aggregated to form antisense foci. Quantification analysis revealed the percentage of antisense foci-positive cells was as high as 23.4% ± 4.2% among sense foci-negative cells, reflecting the inversion rate of paired SaCas9 gRNAs. These events are schematically illustrated in Figure 3E.

Targeted Insertion of PolyA Signals in 3′ UTR Upstream of Expanded CTG Repeats Led to the Elimination of Intranuclear RNA CUG Repeat Foci and the Reversal of Aberrant Alternative Splicing

We have thus developed an approach that allows the insertion of PolyA signals upstream of expanded CTG repeats, which should prematurely terminate transcription and eliminate expanded RNA CUG repeats. The ideal PolyA signal insertion site is in the 3′ UTR upstream of the CTG repeats, which generates an engineered DMPK mRNA without CUG repeats (Figures 4A and 4B). To increase the specificity of targeted insertion of PolyA signals, we adopted the SpCas 9 nickase system.[23–25] SpCas9 D10A nickase is created by an aspartate-to-alanine substitution (D10A) in the RuvC I domain of SpCas9[23,25,26] that can produce a nick guided to a specific genome site using a sequence-specific gRNA. The single nick in the genome is typically repaired either seamlessly via the single-strand break repair pathway or through high-fidelity homology-directed repair (HDR) when an ectopic donor exists.[27] However, when there is an adjacent nick on the opposite strand from the second gRNA-SpCas9 nickase, it can cause double-strand breaks. These double-strand breaks are repaired preferentially by HDR when a donor exists, which allows the insertion of ectopic DNAs. The double-strand break is relatively more specific due to the requirement of more than double the length of DNA recognition sequence compared to the single wild-type SpCas9. We found that one pair of SpCas9g gRNAs (Sp870/Sp870U) facilitated the insertion of PolyA signals in the 3′ UTR upstream of the CTG repeats. The targeting efficiency increased by increasing the total length of homologous arms, but a minimum of 281 bp (5′ arm 97 bp, 3′ arm 184 bp) was sufficient to induce HDR (Figure S4). The introduction of PolyA signals in the 3′ UTR upstream of expanded CTG repeats led to the elimination of nuclear RNA CUG repeat foci in a subset of DM1 NSCs (Figure S5).

To establish a foundation for future personalized cell-based therapies, we used the same strategy to generate genome-edited iPSC clones. We

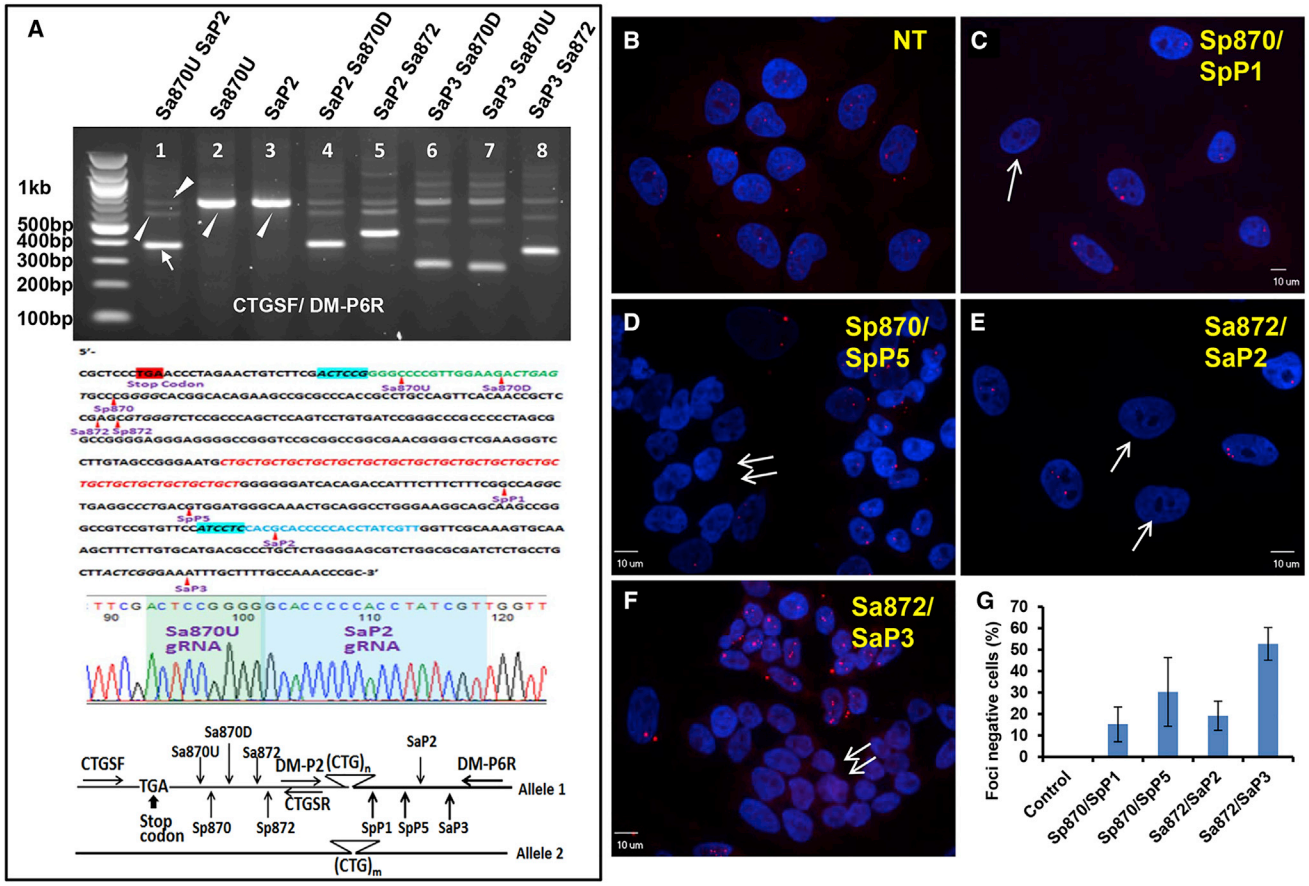

Figure 2. Targeted Deletion of the CTG Repeats by Paired SaCas9 gRNAs Flanking the CTG Repeats

(A) Targeted deletion of the CTG repeats in HEK293 FT cells. Upper panel: transfection of HEK293 FT cells (80% confluent) in 24-well plates with a combination of Sa870D, Sa870U, Sa872, SaP2, SaP3, or single gRNAs with SaCas9-EGFP is shown. Cells were sorted and collected 48 hr after transfection for subsequent PCR analysis using primer CTGSF/DM-P6R. Lane 1 demonstrates high cutting efficiency, which led to a shortened PCR product (arrow). Middle panel: Sanger sequencing showed seamless rejoining. The middle, top PCR products (arrowheads) and PCR products from single gRNA-CRISPR/SaCas9 (arrowheads in lanes 2 and 3) were all sequenced and demonstrated cuts at only one end, and they annealed with random insertion or deletion of nucleotides. Lower panel: schematic illustration shows the 3′ UTR of *DMPK* gene and the location of cut sites for individual SaCas9 gRNAs in 293 genome. (B–G) Targeted deletion of expanded CTG repeats evaluated by loss of intranuclear RNA CUG repeat foci in DM1 NSCs. After transfection of paired SaCas9 gRNAs, DM1 NSCs were sorted for GFP-positive cells, and they were cultured for 72 hr in chamber slides in DMEM supplemented with 2% horse serum prior to RNA FISH. In parental DM1 NSCs derived from DM-03 iPSCs, all the cells contained intranuclear RNA CUG repeat foci (B). Paired Cas9 gRNAs led to the deletion of expanded CTG repeats represented by a subset of cells that lost intranuclear RNA CUG repeat foci (C and E, arrows). Clusters of foci-negative cells were observed in cultures that received paired Cas9 gRNAs (D and F, double arrows). The pictures were taken adjacent to foci-positive cells to show that the foci negativity was not due to a technical issue with the FISH assay. The cutting efficiency calculated by the percentage of cells that lost intranuclear RNA CUG repeat foci was the highest in the Sa872/SaP3 pair (G). Data are represented as mean ± SEM.

screened and isolated a clone that totally lost intranuclear RNA CUG repeat foci compared to parental iPSCs (Figures 4C and 4D) and maintained expression of pluripotent stem cell markers (Figures 4E and 4F). PCR-based genotyping revealed the correct insertion of PolyA signal cassette in the 3′ UTR upstream of the CTG repeats (Figure 5A, upper panel). Triplet repeat primed (TP)-PCR confirmed that the CTG repeat expansion remained (Figure 5A, middle panels). We also performed Southern blot, and it showed the disappearance of the corresponding expanded band due to the introduction of an extra EcoRI site, indirectly confirming the insertion of the PolyA signal cassette (Figure S2). The insertion of the PolyA signals in the 3′ UTR was predicted to generate a new *DMPK* transcript, with an engineered 3′ UTR containing simian virus 40 (SV40) polyA and bovine growth hormone (BGH) polyA signals. To test the stability and the post-transcriptional processing of these *DMPK* transcripts, we performed RT-PCR for *DMPK* isoforms. We found *DMPK* transcripts with engineered 3′ UTRs were stably expressed and processed normally, as reported in wild-type *DMPK* transcripts with inclusion or exclusion of exon 13 and/or 14[28] (Figure 5B; Figures S6A and S6B). To test whether these *DMPK* transcripts could be exported to the cytoplasm and increase the total *DMPK* RNAs, we performed qRT-PCR of DMPK RNA in the cytoplasm in NSCs derived from control,

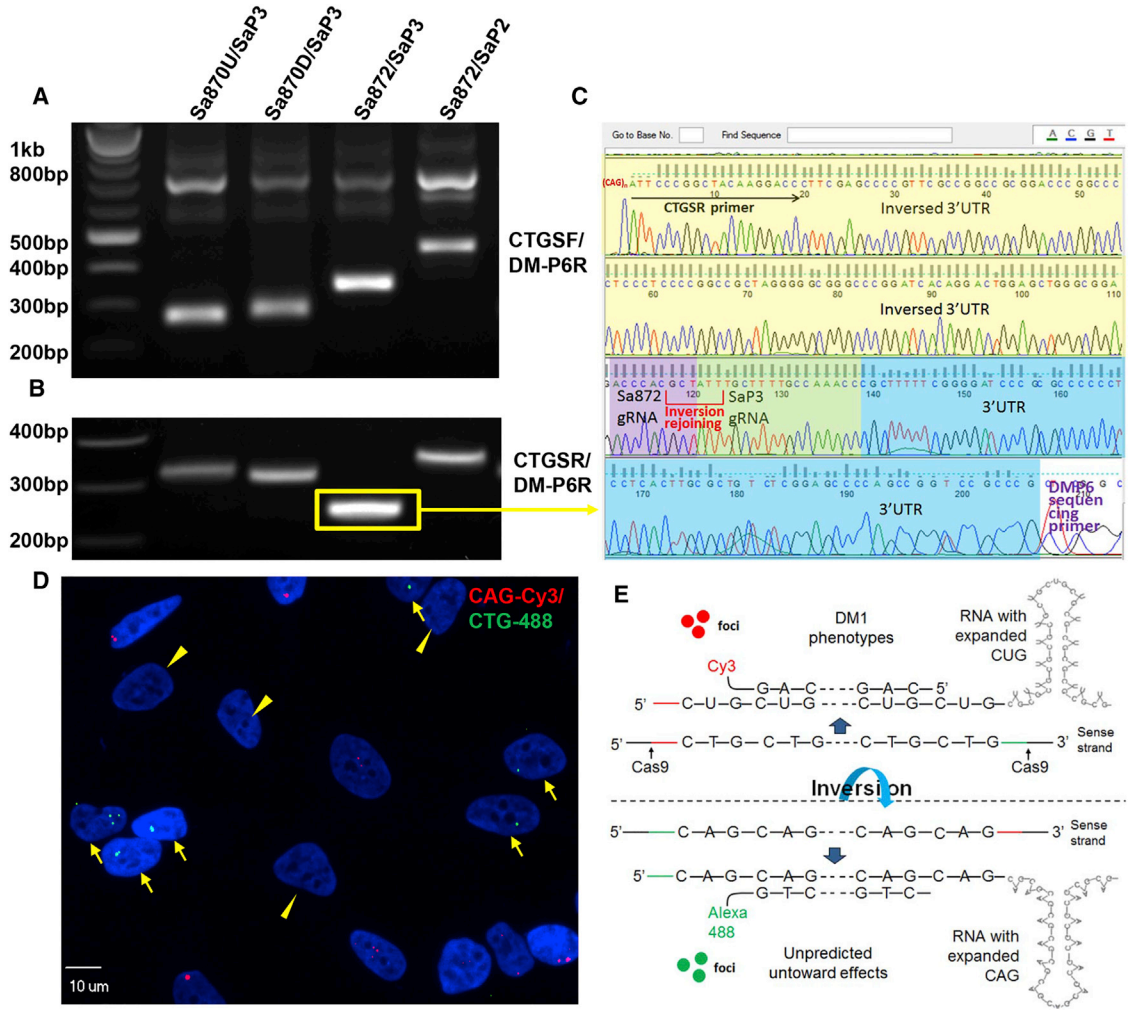

Figure 3. Frequent Inversion of Flanked CTG Repeat Sequence by Paired SaCas9 gRNAs in DM1 NSCs

(A) DM1 NSCs were transfected with each SaCas9 gRNA pair and sorted. Genomic PCR using primer pair CTGSF/DM-P6R generated two PCR products. The lower bands were shortened PCR products from the deletion of flanked sequence using each CRISPR/SaCas9 gRNA pair. (B) Two primers in the same direction (CTGSR/DM-P6) in the DMPK gene generated new PCR products in the DM1 NSCs transfected with SaCas9 gRNA pairs, suggesting inversion of flanked CTG repeats by paired CRISPR/SaCas9 gRNAs. (C) Sanger sequencing of one representative band (boxed) demonstrated the seamless rejoining of the inverted flanking segment (only the end at SaP3 cutting site is shown here). (D) Double FISH using probes specific for CUG repeats (Cy3 labeled) and probes specific for CAG repeats (Alexa 488 labeled) showed mixed cells with nuclei containing sense intranuclear RNA CUG repeat foci (red), antisense RNA CAG repeat foci (green, arrows), or loss of foci (arrowheads). Sense or antisense foci never co-exist in individual cells, and we have never observed antisense foci in untreated DM1 NSCs. (E) Schematic view of consequences of targeted deletion of expanded CTG repeats.

DM1, and genome-edited DM1 iPSCs. We found cytoplasmic DMPK RNA in DM1 NSCs was lower than that of the normal control. The cytoplasmic DMPK RNA significantly increased in the NSCs derived from the genome-edited J-6 iPSCs (Figure 5C).

The incorporation of the PolyA signal cassette did not affect pluripotency, as the genome-edited human DM1 iPSC clone expressed pluripotent stem cell markers (Figures 4E and 4F) and could be differentiated into cardiomyocytes and NCSs, which all showed loss of intranuclear RNA CUG repeat foci and reversal of alternative splicing (Figure 6). Cardiomyocytes derived from genome-edited DM1 iPSCs demonstrated spontaneous contractions similar to wild-type cardiomyocytes (Video S1). NSCs were further differentiated into forebrain neurons, and again they showed the loss of intranuclear RNA CUG repeat foci and reversal of known aberrant alternative splicing of *MAPT*, *MBNL1*, *MBNL2*, *SERCA1*, and *INSR* (Figure S7).

Skeletal muscle is the most affected tissue in DM1 mainly due to the high expression of mutant *DMPK* transcripts.[29,30] We next investigated whether the insertion of PolyA signals in the 3′ UTR upstream of the CTG repeats could eliminate intranuclear RNA CUG repeat foci in DM1 iPSC-derived skeletal muscle myofibers. We first adopted a forced-induction protocol with transfection of key factors using a commercial kit (QuickMuscle Skeletal SeV kit, Elixirgen, Baltimore,

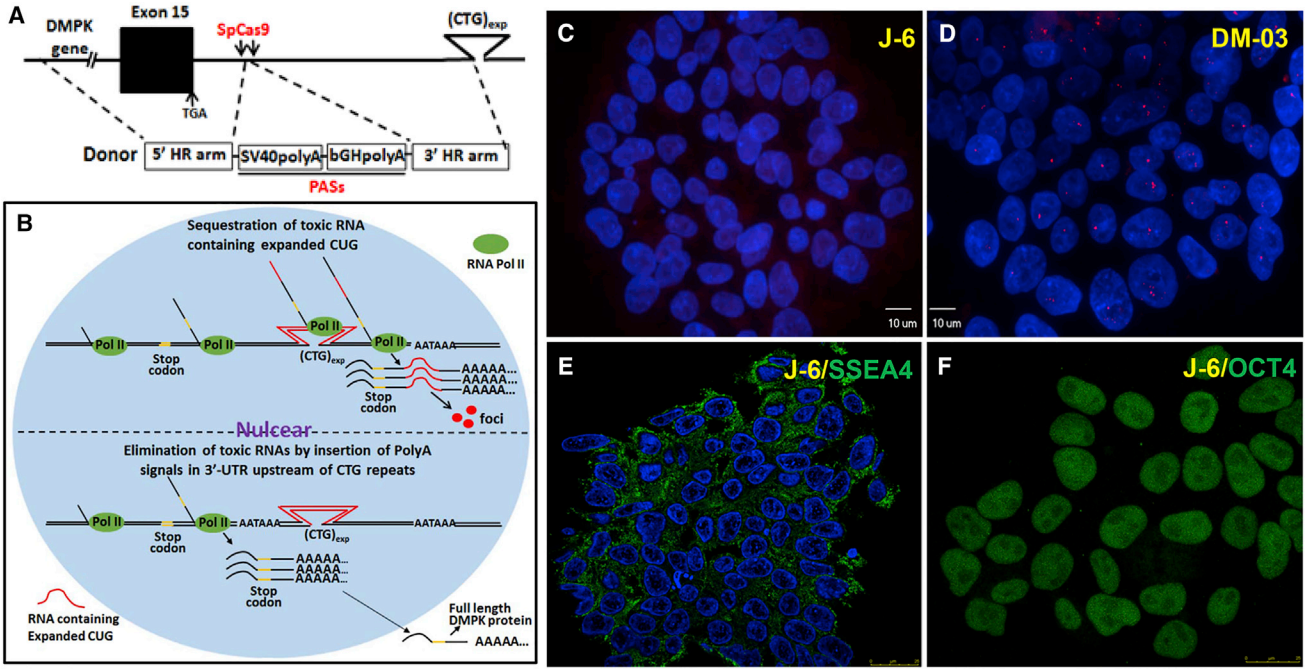

Figure 4. Targeted Insertion of PolyA Signals in the 3′ UTR Upstream of Expanded CTG Repeats for the Elimination of Toxic Expanded RNA CUG Repeats
(A) Schematic overview of targeted insertion of PolyA signals (SV40polyA-BGHpolyA, 350 bp) upstream of the CTG repeats in the 3′ UTR of *DMPK*. Insertion is predicted to be mediated by paired gRNAs and SpCas9 nickase. (B) Schematic view of the genome-editing process and the expected results. (C) Genome-edited DM1 iPSC clone (J-6) showed a complete loss of intranuclear RNA CUG repeat foci in each cell within a colony that may be derived from a single clone. (D) Unmodified parental DM1 iPSCs (DM-03) showed intranuclear RNA CUG repeat foci. (E and F) Immunofluorescent staining showed the expression of pluripotent stem cell markers (E, SSEA4 and F, OCT4) in genome-edited J-6 clone.

MD, USA). The resultant terminally differentiated myofibers from genome-edited J-6 iPSCs showed a complete loss of intranuclear RNA CUG repeat foci (Figures S8A–S8D). However, this protocol was designed for terminal differentiation and the medium formulation is proprietary. To move this therapeutic editing into clinical application for personalized cell-based cell therapy, we tested a chemically defined protocol[31] to obtain skeletal muscle progenitor cells. We were able to obtain PAX3^{+} and PAX 7^{+} skeletal muscle progenitor cells with the loss of intranuclear RNA CUG repeat foci (Figures S8E–S8H). Under this chemically induced condition, the genome-edited iPCSs were able to be differentiated into skeletal muscle myofibers *in vitro*, which also showed the loss of intranuclear RNA CUG repeat foci (Figure 7).

DISCUSSION

DM1 is caused by expanded CTG repeats in the 3′ UTR. It is conceivable that simply deleting the expanded CTG repeats may cure the disease. With the advancement of therapeutic genome-editing technologies, this is becoming more realistic. In this study, we found that paired SpCas9 gRNAs flanking the CTG repeats led to targeted deletion of the repeats. However, the efficiency was insufficient for direct clinical applications. In addition, SpCas9 is too large to be packaged into AAV for clinical use. We then examined the smaller SaCas9 that can be packaged to an AAV vector along with a gRNA sequence. In our results, the cutting efficiency varied among each pair of gRNA-Cas9. Multiple factors could have affected the cutting efficiency, including gRNA specificity, gRNA location relative to the CTG repeats, and the level of Cas9 expression. As it was not the purpose of this study to find an algorithm to optimize these parameters, we screened gRNA pairs to find an SaCas9 gRNA pair with relatively higher efficiency for targeted deletion of the CTG repeats. Unexpectedly, we found that the SaCas9 gRNA pairs caused frequent inversion of expanded CTG repeats in DM1 NSCs. The inversion caused the transcription of *DMPK* gene with expanded RNA CAG repeats. Inversion of a segment of mammalian genome by CRISPR with two gRNAs was a frequent event, as reported before.[32]

The deleterious effects of the inversion of CTG repeats in the *DMPK* gene and the resulting expanded RNA CAG repeats remain undetermined, but repeat-associated non-AUG translation[33–36] is a significant concern. Repetitive RNA motifs can initiate translation in the absence of an AUG start codon. The translation can initiate in multiple reading frames, generating homopolymeric proteins with glutamine, serine, or alanine for CAG repeats. These homopolymeric proteins are generally considered toxic and account for neurodegeneration.[37–44] Clearly, the issue of haploinsufficiency of *DMPK* in DM1[45–49] is not resolved when the inversion happens and the expanded RNA CAG repeats are sequestrated in the nuclei and form intranuclear RNA foci. Other genome anomalies have been reported using single or double CRISPR/Cas9 cleavage adjacent to the

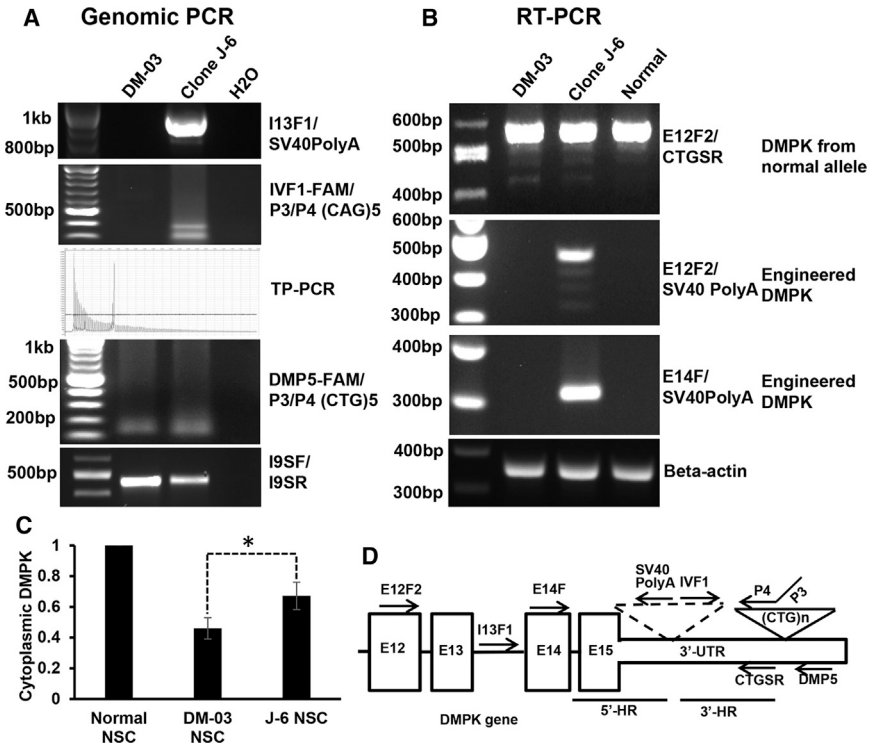

Figure 5. Correct Insertion of PolyA Signals in the 3′ UTR Upstream of Expanded CTG Repeats and Normal Processing of *DMPK* Transcripts

(A) Genotyping by junctional PCR and TP-PCR showed the correct insertion of the PolyA cassettes in the 3′ UTR. Junctional PCR product was confirmed by Sanger sequencing (data not shown). TP-PCR from IVF1-FAM/P3/P4 $(CAG)_5$ further confirmed the insertion of the cassette in the 3′ UTR upstream of the CTG repeats and the presence of the expanded CTG repeats. TP-PCR from DMP5-FAM/P3/P4 $(CTG)_5$ further confirmed the presence of expanded CTG repeats and the identity of clone J-6 from parental DM-03 iPSC. (B) RT-PCR showed the expression of normal *DMPK* transcripts in clone J-6, suggesting that the normal allele was not affected. PCR products from E12F2/SV40PolyA showed the edited *DMPK* mRNA with SV40PolyA in the J-6 clone had the same splicing pattern as wild-type *DMPK* mRNA. Both the top and bottom bands of the wild-type *DMPK* and *DMPK* with SV40PolyA were verified by Sanger sequencing, and both showed the inclusion or exclusion of exons 13 and 14 (see also Figures S6A and S6B). (C) qRT-PCR of cytoplasmic *DMPK* RNA showing significantly increased cytoplasmic *DMPK* RNA in NSCs derived from genome-edited J-6 iPSCs compared to parental DM-03-derived NSCs. *$p < 0.01$ by Student's t test. (D) Schematic view of primer positions.

CTG repeats.[10] van Agtmaal et al.[10] found that single double-strand breaks (DSBs) near a long CTG induced random loss of the CTG repeats, including the loss of the CTG repeats in entirety, which could be potentially used to generate isogenic cell lines. However, its use in therapeutic development could be difficult due to the random and uncontrollable nature of the CTG repeat loss. Using dual CRISPR/Cas9-directed cleavage, the authors reported equal excision efficiency between wild-type and long-expanded DMPK alleles. Frequent inversion of the wild-type allele was reported, but the inversion of the expanded allele was not examined. Our current study provided evidence that frequent inversion also occurs in the expanded allele.

For cell-based therapy using a single or dual CRISPR/Cas9 cleavage approach, clonal selection followed by propagation of correctly edited iPSCs is necessary. The cloning process could be difficult due to the lack of selective markers. The use of two CRISPR/Cas9 guides also increased the possibility of off-target effects. Additionally, the repair of DSBs induced by CRISPR/Cas9 often leads to deletions extending many kilobases upstream or downstream of the DSBs,[50] which could potentially affect the expression of the *DMPK* gene. We caution the use of this approach for *in vivo* therapeutic genome editing. This may also apply to other microsatellite repeat expansion-mediated neurodegenerative disorders.

Given these findings, we pursued an alternative approach to therapeutic genome editing by inserting PolyA signals in the 3′ UTR upstream of the CTG repeats via HDR. Using this method, RNA polymerase II is expected to prematurely terminate transcription following the engineered PolyA site, which will generate *DMPK* pre-mRNA with all exons and lack the expanded CUG repeats that define mutant *DMPK*. We have found the post-transcription procession of these mRNA precursors is very similar to the wild-type *DMPK*. This is particularly important for *in vivo* therapeutic development, as the *DMPK* function would not be affected even if both the mutant and the normal allele were targeted. We have found the elimination of toxic RNA CUG repeat foci and reversal of alternative splicing in differentiated neural stem cells, cardiomyocytes, and skeletal muscle myofibers. This approach not only eliminated the toxic CUG repeats but also released newly engineered *DMPK* transcripts into the cytoplasm, which could potentially offset abnormalities that are caused by haploinsufficiency.[45–49]

We have shown that the expanded CTG repeats remained in the genome-edited clone and its progenies. However, we have not tested whether the current approach could induce the same spontaneous contraction of expanded CTG repeats as reported in the recent publication after single cleavage by CRISPR/Cas9.[10] How the existence of a donor with homologous arms and the adoption of the CRISPR/Cas9 nickase system affect this process remain undetermined.

The direct clinical application for this type of therapeutic genome editing will be the development of personalized cell-based therapy. The idea is to generate patient-specific iPSCs from DM1 patient fibroblasts, edit the genome in these iPSCs to stop the production of the toxic RNA

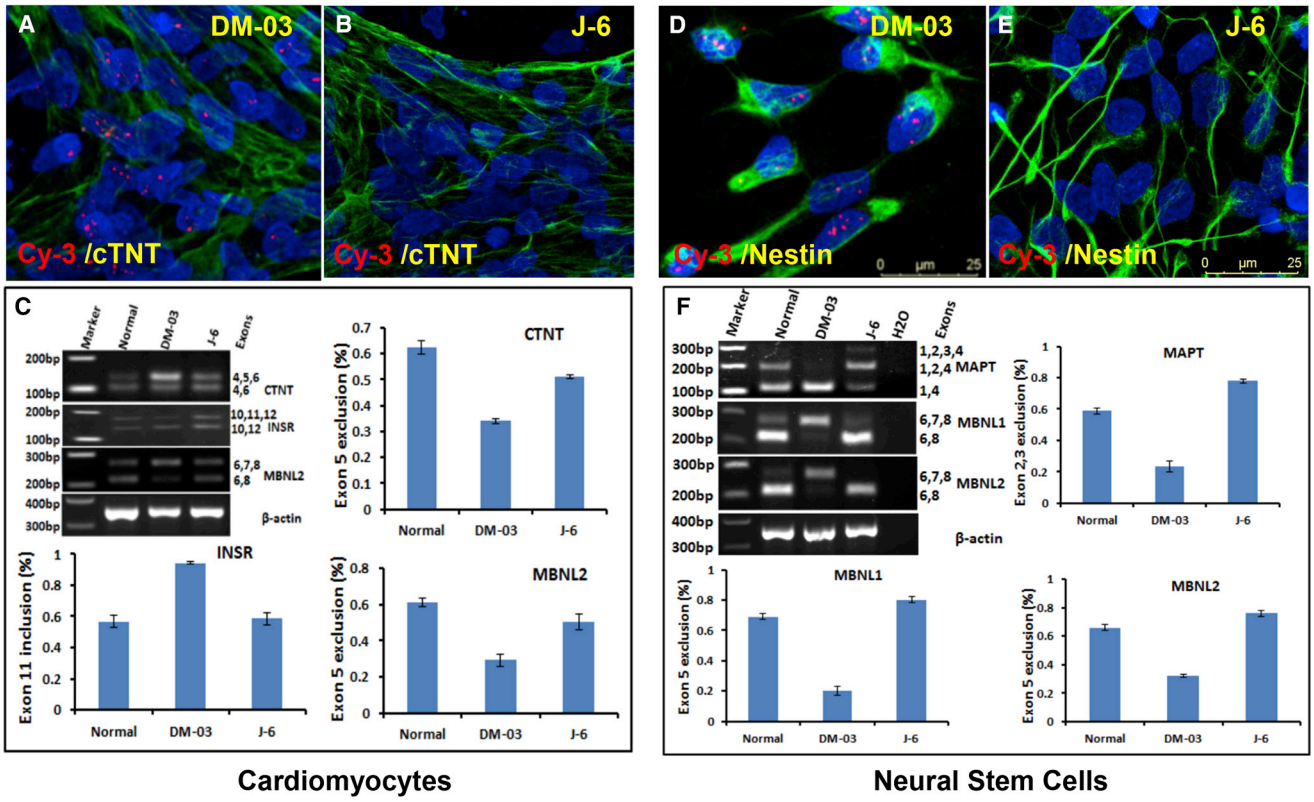

Figure 6. The Insertion of the PolyA Signals in 3′ UTR Upstream of the Expanded CTG Repeats in DM1 iPSCs Led to the Elimination of Intranuclear RNA CUG Repeat Foci and the Reversal of Abnormal Splicing in Linear-Differentiated Cardiomyocytes and NSCs

(A) Intranuclear RNA CUG repeat foci were only detected in cardiomyocytes derived from parental DM-03 iPSCs. (B) No foci were detected in cardiomyocytes derived from genome-edited J-6 iPSCs. (C) Agarose gel images and quantitative analyses showed the reversal of the aberrant splicing pattern in *CTNT*, *INSR*, and *MBNL2* in cardiomyocytes. (D) Intranuclear RNA CUG repeat foci were only detected in NSCs derived from parental DM1 iPSCs (DM-03). (E) No foci were detected in the NSCs derived from genome-edited J-6 iPSCs. (F) Agarose gel images and quantitative analyses showed the reversal of the aberrant splicing pattern in *MAPT* and *MBNL1*, *2* in NSCs. *CTNT*, cardiac troponin T; *INSR*, insulin receptor; *MBNL1*, *2*, muscleblind-like 1, 2; *MAPT*, Microtubule-associated protein tau. Data are represented as mean ± SEM.

CUG repeats, differentiate these genome-edited iPSCs into skeletal muscle progenitor cells, and then transplant skeletal muscle progenitor cells back to the same patient. Cell transplantation as a treatment for muscular dystrophy was previously tested on Duchenne muscular dystrophy patients. The results were disappointing. The main issue was the source of the transplanted cells. Earlier studies used allogenic myoblasts derived from muscle biopsy tissues. The initial immune reaction eliminated 75%–80% of the transplanted cells.[51–57] Additionally, myoblasts have their own intrinsic defects for application in cell-based therapies. Myoblasts were acquired from *in vitro* cultures of isolated satellite cells from muscle tissues. These myoblasts can only proliferate for a limited number of passages, and further *ex vivo* expansion degrades their myogenic capacity.[58] Upon transplantation, surviving myoblasts migrated poorly and failed to replenish the satellite compartment; their effect could not be sustained.[58,59]

We have shown here that DM1 iPSCs and genome-edited iPSCs were able to differentiate into skeletal muscle progenitor cells. The advantage of iPSCs is the prospect of generating unlimited quantities of specific cell populations for regenerative purposes. iPSCs are derived from somatic cells and do not involve the use of embryos, which reduces ethical concerns. iPSCs generated from the same patient, termed patient-specific iPSCs, can theoretically avoid immune rejection.[60–62] We anticipate that genome-edited skeletal muscle progenitor cells can function as postnatal/immature satellite cells that self-renew to replenish the satellite compartment upon transplantation and give rise to myofibers. This approach may also be applied to *in vivo* therapeutic genome editing.

There are some limitations to this approach, however. First, this approach will not solve the antisense transcription and repeat-associated non-AUG translation from the antisense transcripts of the expanded repeat.[33] However, in the current study, we did not observe the antisense transcription in the double FISH studies in the parental DM1 cells as what we found when there was an inversion of the expanded repeats, suggesting the transcription of the DM1-antisense gene is relatively low or absent. This was also confirmed by a recent publication in which DM1 antisense transcript abundance remained very low in all tissues analyzed.[63] Second, the expanded CTG repeats in the *DMPK* gene were not removed, which have been shown to

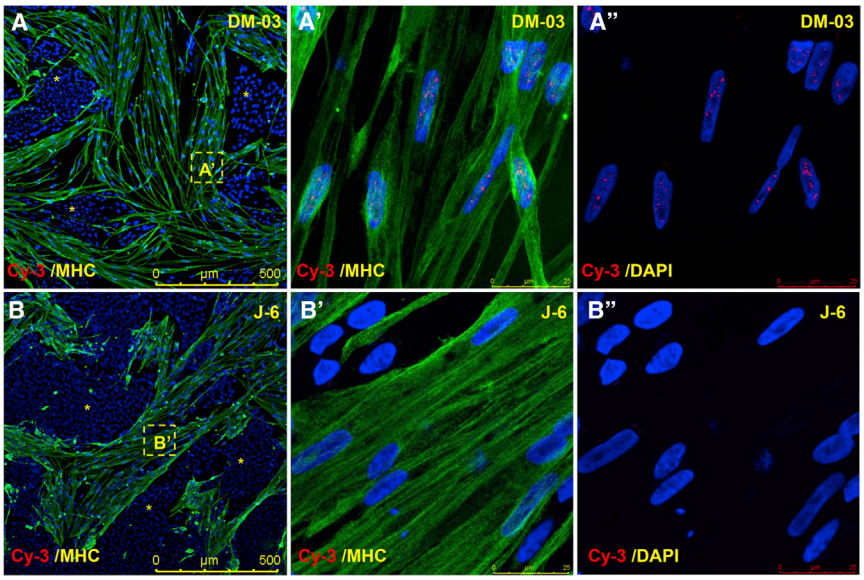

Figure 7. The Insertion of the PolyA Signals in the 3′ UTR Upstream of the Expanded CTG Repeats in DM1 iPSCs (DM-03) Led to the Elimination of Intranuclear RNA CUG Repeat Foci in Linear-Differentiated Skeletal Muscle Myofibers (30 Days after Differentiation)

(A–A'') Skeletal muscle differentiation from parental DM1 iPSCs. Myofibers expressing MHC (A and A', green) demonstrated the presence of RNA CUG repeat foci accumulated in the nuclei (A' and A''). (B–B'') Skeletal muscle differentiation from genome-edited J-6 iPSCs. Myofibers expressing MHC (B and B', green) showed an absence of RNA CUG repeat foci were eliminated in the nuclei (B' and B''). The differentiation was not homogeneous and there were undifferentiated cells or non-myogenic cells present in the culture (*in A and B).

affect transcription of adjacent genomic regions (DMAHP/SIX5 gene).[64–67] Heterozygous and homozygous mice for *Six5* deletion developed premature cataracts.[68,69] However, the homozygous mutant mice for *Six5* had no apparent abnormalities of skeletal muscle function.[68] We have created isogenic human DM1 cellular models, which may be a better proxy for understanding the molecular mechanisms of DM1 in the human cells. Regardless, the complete reversal of alternative splicing after genome editing in NSCs, neurons, and cardiomyocytes using this approach suggests the correction is sufficient to correct the aberrant events caused by the expanded CTG repeats. Furthermore, the findings in this study support the primary role of the expanded CUG RNA repeats on disease pathogenesis.[70,71]

In summary, paired gRNA-CRISPR/Cas9 caused frequent inversion of expanded CTG repeats at the *DMPK* locus, and this approach was not suitable for *in vivo* therapeutic genome editing. Targeted insertion of PolyA signals into the 3′ UTR, upstream of expanded CTG repeats, is a viable approach for the development of therapeutic genome editing for DM1.

MATERIALS AND METHODS

Construction of gRNA-CRISPR/Cas9 Plasmids

All the sequences for the paired single-stranded DNA oligonucleotides are listed in Table 1. Single-stranded DNA oligonucleotides for gRNAs of SpCas9 were designed following guidelines in GeneArt CRISPR Nuclease Vector Kit (1750624, Invitrogen, Carlsbad, CA, USA) and synthesized by Integrated DNA Technologies (IDT, Coralville, IA, USA). Potential off-targets were predicted by recently published software.[72] Only gRNAs that had the fewest targets in the coding region were selected for screening of targeted deletion. gRNA for SpCas9 was inserted into a CRISPR nuclease vector containing OFP according to the manufacturer's protocol. Plasmid DNA was sequenced using U6 forward primers. Single-stranded DNA oligonucleotides of gRNAs for SaCas9 with a BsaI overhang were synthesized by IDT. To increase the cutting efficiency, guanosine nucleotide was added to the 5′ end. The annealed double-stranded oligonucleotides were cloned into the BsaI site of the PX601 plasmid (61591, Addgene). The SpCas9 nickase vector was obtained from Sigma (CAS9D10AP-1EA).

Verification of gRNA by SURVEYOR Cleavage Detection Assay

HEK293 FT cells were transfected with single gRNA and SpCas9 engineered in one plasmid with an OFP reporter (GeneArt, Life Technologies), or single gRNA and SaCas9 were transfected along with a GFP-reporting plasmid in a 24-well plate. 48 hr after transfection, genomic DNA was extracted after sorting OFP- or GFP-positive cells and subjected to PCR with primers flanking the gRNA-binding sites for SURVEYOR assay, using the GeneArt Genomic Cleavage Detection Kit (1742677, Invitrogen, Carlsbad, CA, USA). Briefly, 1×10^6 cells were obtained for DNA extraction using cell lysis buffer and protein degrader, followed by incubation (68°C 15 min, 95°C 10 min, and 4°C hold) in a thermal cycler. The PCR reaction was run with the following conditions: enzyme activation at 95°C for 10 min, and then 40 cycles of denaturation at 95°C for 30 s, annealing at 58°C for 30 s, extension at 72°C for 30 s, followed by final extension at 72°C for 7 min. Primers were CTGSF/CTGSR for upstream gRNA-CRISPR/Cas9, and DM-P2/DMP-6R for downstream gRNA-CRISPR/Cas9. 3 μL PCR product was used to set up a denaturing and re-annealing reaction using the following program: 95°C 5 min, 95°C –85°C (−2°C/s), 85°C–25°C (−0.1°C/s), and 4°C. Finally, 1 μL detection solution containing Surveyor nuclease was added to the reaction and incubated at 37°C for 1 hr. The reaction product was then separated on 1.6% agarose gel to detect cleavage.

Construction of Homologous Recombination Donor Vector Containing PolyA Signal Cassette

The vector map is shown in Figure S9. AAV2-MCS2 vector (6954, Addgene) was used as a backbone vector. The insertion cassette, which contained the PolyA signals and selectable GFP marker

Table 1. gRNA Sequences and Location within the 3 UTR

gRNA	Target Sequence in the *DMPK* Gene (5′→3′)[a]	Cutting Sites
Sp870	GTTGGAAGACTGAGTGCCCG *GGG*	175 bp upstream of the beginning of the CTG repeats
Sp870U	CGGAGTCGAAGACAGTTCT*A GGG*	216 bp upstream of the beginning of the CTG repeats
Sp872	TTCACAACCGCTCCGAGCGT *GGG*	119 bp upstream of the beginning of the CTG repeats
Sp872U	GCGGCTTCTGTGCCGTGCCCC *GGG*	169 bp upstream of the beginning of the CTG repeats
Sp872V	CGGGCACTCAGTCTTCCAAC *GGG*	189 bp upstream of the beginning of the CTG repeats
SpP1	ACCATTTCTTTCTTTCGGCC *AGG*	29 bp downstream of the end of the CTG repeats
SpP5	GCAGTTTGCCCATCCACGTC A*GG*	48 bp downstream of the end of the CTG repeats
Sa872	CAGTTCACAACCGCTCCGAGC *GTGGGT*	121 bp upstream of the beginning of the CTG repeats
Sa870U	CTCAGTCTTCCAACGGGGCCC *CGGAGT*	196 bp upstream of the beginning of the CTG repeats
Sa870D	CTCCGGGGCCCCGTTGGAAGA *CTGAGT*	186 bp upstream of the beginning of the CTG repeats
SaP2	AACGATAGGTGGGGGTGCGTG *GAGGAT*	112 bp downstream of the end of the CTG repeats
SaP3	GGTTTGGCAAAAGCAAATTTC *CCGAGT*	214 bp downstream of the end of the CTG repeats

[a]The NGG sequence for SpCas9 and the NNGRRT sequence for SaCas9 are also listed.

followed by a 2A self-cleaving peptide and puromycin resistance gene, was assembled using standard cloning techniques. Site-specific insertion was mediated by incorporating homologous arms flanking the insertion cassette. 5′-homologous arms (500 bp) were PCR amplified using high-fidelity DNA polymerase (Platinum Pfx DNA Polymerase, Invitrogen, Carlsbad, CA, USA), and a 3′-homologous arm (183 bp) was synthesized by GenScript (Piscataway, NJ, USA). Two single gRNA transcription units were also synthesized and cloned upstream of the 5′-homologous arm. The whole cassette was cloned between NheI and MluI sites of the AAV2-MCS2 vector. This donor was used in this study for the generation of iPSC clones. The puromycin coding sequencing can be removed by BsiWI without affecting the GFP expression to generate a donor so that the remaining cassette (3.71 kb) flanked by inverted terminal repeats (ITRs) can be packaged to AAV for *in vivo* application and the expression of GFP can be tracked for transduction efficiency. An EcoRI cut site was included in the cassette, which changed the pattern of the expanded allele in Southern blot.

Cell Lines and Maintenance

The HEK293 FT cell line was from the laboratory of N.T. The normal control iPSC and the DM1 iPSC (DM-03) lines in this study were established in our lab.[21] DM1 NSCs were differentiated from the DM-03 iPSC cell line and have been adapted to 20% fetal bovine serum (FBS) in DMEM, as previously reported.[22] When cultured in 2% horse serum for 72 hr, all the cells contained intranuclear RNA CUG repeat foci. Thus, the percentage of NSCs that have lost intranuclear RNA CUG repeat foci after genome manipulation can be viewed as the targeting efficiency.

Transfection of HEK293 FT Cells

HEK293 FT cells were transfected with CRISPR/Cas9 using Lipofectamine LTX Reagent with PLUS Reagent (15338100, Thermo Fisher Scientific, Grand Island, NY, USA). Briefly, HEK293 FT cells were plated into a 24-well plate. 750 ng plasmid was added to 50 μL Opti-MEM reduced serum medium (Thermo Fisher Scientific, Grand Island, NY, USA). Then 0.75 μL PLUS reagent was added, mixed, and incubated at room temperature for 5 min. 3 μL Lipofectamine in 50 μL Opti-MEM was then added and incubated at room temperature for 5 min. 100 μL DNA-lipid was added to one well. Transfection solution was distributed gently by moving the plate back and forth. Cells were harvested and sorted 48 hr later.

Transfection of DM1 NSCs

DM1 NSCs were transfected at 80% confluence in a 6-well plate with gRNA-CRISPR/Cas9 using Lipofectamine LTX Reagent with PLUS Reagent. Briefly, 3 μg gRNA plasmid was added to 150 μL Opti-MEM reduced serum medium. Then 3 μL PLUS reagent was added, mixed, and incubated at room temperature for 5 min. 12 μL Lipofectamine in 150 μL Opti-MEM was then added and incubated at room temperature for 5 min. 300 μL DNA-lipid was added to one well. Transfection solution was distributed gently by moving the plate back and forth. Cells were harvested and sorted 72 hr later. OFP- or GFP-positive cells were seeded onto ibidiTreat μ-slides (Ibidi, Martinsried, Germany) and cultured in DMEM 20% FBS medium overnight and then switched to DMEM supplemented with 2% horse serum for 72 hr prior to FISH. The remaining OFP- or GFP-positive cells were seeded back onto a 12-well plate and expanded to a 6-well plate for DNA and RNA extraction.

DM1 iPSC Transfection and Clone Selection

For transfection, DM1 iPSCs (DM-03) were passed as small colonies using Gentle Cell Dissociation Reagent (STEMCELL Technologies) the day before transfection on a Vitronectin-coated 6-well plate in mTeSR-E8 medium (STEMCELL Technologies). Transfection was conducted with Lipofectamine LTX Reagent with PLUS Reagent as described above. Briefly, 1 μg of each donor vector and SpCas9 D10 A plasmid was mixed with 3 μL plus reagent and then with 12 μL

Lipofectamine. They were incubated at room temperature for 5 min and then the complex was added dropwise to 1 well of cultured cells in a 6-well plate (2 mL in each well). Medium was changed 24 hr later. Puromycin selection was started 48 hr after transfection at 0.4 μg/mL. Selection was continued until individual clones were large enough for isolation. The GFP-positive and puromycin-resistant clones were selected and subjected to FISH. Intranuclear RNA CUG foci-negative clones were identified for further characterization.

Neural Differentiation, Cardiomyocyte Differentiation, and Skeletal Muscle Differentiation

Neural differentiation and cardiomyocyte differentiation were performed as described previously.[19,21] For forebrain neuron differentiation, cryopreserved NSCs were thawed and cultured in STEMdiff Neural Progenitor Medium (08560, STEMCELL Technologies). On day 0, NSCs were resuspended in 5 mL complete Neural Progenitor Medium and seeded onto a pre-warmed 6-well plate coated with Poly-L-Ornithine and laminin at a density of 5×10^4 cells/cm^2 in complete Neural Progenitor Medium. On day 1, medium was replaced with 2 mL complete STEMdiff Neuron Differentiation Medium (8500, STEMCELL Technologies). For the next 7 days, medium was changed every other day with warm (37°C) complete STEMdiff Neuron Differentiation Medium. On day 7, cells reached 90%–95% confluence and became neuronal precursors. Neuronal precursors were detached with Accutase (STEMCELL Technologies) and seeded onto pre-warmed (37°C) 6-well plates and ibidiTreat μ-slides (Ibidi, Martinsried, Germany) coated with Poly-L-Ornithine and laminin at a density of 2×10^4 cells/cm^2 in complete STEMdiff Neuron Maturation Medium (8510, STEMCELL Technologies). Neurons were allowed to mature for 2 weeks and then subjected to FISH, immunofluorescence (IF), and RNA extraction for RT-PCR.

Skeletal muscle differentiation was first performed by a quick induction method (7 days) according to the manufacturer's protocol (QMS-SeV, Elixirgen Scientific, Baltimore, MD, USA), which is based on a published technology of ectopic expression of a demethylase (JMJD3) and a linear-defining transcription factor (MYOD1).[73] This protocol generated a high percentage of myosin-positive myocytes in 7 days. To isolate skeletal muscle progenitor cells, we adopted a chemically defined induction protocol according to a recent publication,[31] with some modification. Briefly, iPSCs were harvested by TrypLE treatment at 37° for 7 min and resuspended as single cells in mTeSR E8 medium supplemented with 10 μM Rock inhibitor (Y-27362). 2.8×10^5 iPSCs were plated into 6-well plates and 8-well chamber slides coated with Matrigel (Corning Life Sciences). We initiated differentiation when the wells reached 20% confluency using sequential induction with WNT activator (4423, CHIR99021, 3 μM, Tocris Bioscience), BMP inhibitor (04-0074, LDN193189, 0.5 μM, Stemgent), fibroblast growth factor 2 (FGF2, 450-33, 20 ng/mL, PeproTech), hepatocyte growth factor (HGF, 315-23, 10 ng/mL, PeproTech), and insulin-like growth factor 1 (IGF-1, 250-19, 2 ng/mL, PeproTech). On day 20, skeletal muscle progenitor cells in 6-well plates were isolated by TrypLE and 0.05% trypsin and EDTA treatment of the wells and cultured in Matrigel-coated 8-well plates in Skeletal Muscle Cell Growth Media (SKGM-2, CC-3245, Lonza). The expression of skeletal muscle progenitor cell markers (PAX 3 and PAX7) was monitored by IF staining. On day 30, differentiation in 8-well chamber slides was subjected to FISH and IF for myosin heavy chain (MHC).

DNA or RNA Isolation, Genomic PCR, RT-PCR, TP-PCR, and Alternative Splicing Assays

Genomic DNA was isolated with the DNeasy Blood & Tissue Kit (QIAGEN, Valencia, CA, USA). Total RNA was isolated using Quick-RNA MiniPrep (R1055, Zymo Research, Irvine, CA, USA), according to the manufacturer's protocol. Reverse transcription, PCRs, and alternative splicing assays were performed as described previously.[19,20] Primer sequences and PCR conditions can be found in our earlier publications.[19,20] Primers for sarcoplasmic and endoplasmic reticulum Ca^{2+} ATPase 1(SERCA1) are SERCA1-F, 5′-CTCA TGGTCCTCAAGATCTCAC-3′ and SERCA1-R, 5′-AGCTCTGCC TGAAGATGTGTCAC-3′. The intensity of each band on electrophoresis gel image was analyzed by Alphaview software (ProteinSimple, San Jose, CA, USA). The percentage of exon inclusion or exclusion was calculated from three independent PCR experiments.

Cytoplasmic RNA Isolation and qRT-PCR

Quantitation of cytoplasmic *DMPK* RNA was performed by qRT-PCR in early passages of NSCs derived from parental DM1 and genome-edited J-6 iPSC clones. The RNA isolation and the subsequent qRT-PCR reactions were performed according to the Minimum Information for Publication of Quantitative Real-Time PCR Experiments (MIQE) guidelines. Cytoplasmic RNA extraction was performed using the Cytoplasmic & Nuclear RNA Purification Kit (Norgen Biotek, Thorold, Canada). Single-stranded cDNA was synthesized from 100 ng total RNA using SuperScript III First-Strand Synthesis System (Thermo Fisher Scientific), following the manufacturer's instructions. PCR amplifications were carried out in a total volume of 25 μL, containing 12.5 μL 2× Applied Biosystem SYBR Green PCR Master Mix (Thermo Fisher Scientific), 2.5 μL cDNA (10 ng), 2.25 μL primer (10 μM), and 5.5 μL water on a Bio-Rad CFX96 Deep Well Real-Time System (Bio-Rad, USA). Amplification efficiency of environmental DNA can be assessed by determining the threshold cycle (Ct) for different amounts of the DNA sample. Relative quantification allows calculation of the ratio between the amount of target template and a reference template in a sample. The cytoplasmic *DMPK* RNA was normalized to *ACTIN* RNA within the same sample to determine ΔCt. The cytoplasmic *DMPK* RNA in unmodified DM1 NSCs or J-6 NSCs was presented as the fold changes relative to normal control NSCs. Statistical analysis was performed by Student's t test using the SPSS version 11.0 statistical software package.

Southern Blot

Southern blot was performed as described before.[19,74] Briefly, 8 μg total genome DNA was digested with EcoRI and subjected to 0.8% agarose gel electrophoresis and blotting to Nylon membrane. After UV crosslink, the member was subjected to hybridization and

detection using probes labeled with α-^{32}P-dCTPs. The primers used to generate the template for probe labeling were DMPK1A, 5′-GCAAAGTGCAAAGCTTTCTTGTGCATGAC-3′ and DMPK1B, 5′-GGTCCTAGGTGGGGACAGACAATAAATACC-3′, which makes a 307-bp probe targeting *DMPK* gene downstream of the CTG repeats. Radioactive signal was visualized on X-ray film after 2 days of exposure at −80°C.

IF Staining, FISH, and Double FISH

IF staining and RNA-FISH were performed as described previously.[20,21] Antibodies (Pax 3-c, Pax7-c, Myosin heavy chain [MF20-C], Titin, and Myogenin [F5-c]) for skeletal muscle differentiation were all from the Developmental Studies Hybridoma Bank (Iowa City, IA, USA). Each antibody was used at a dilution of 1:200. Double FISH was performed sequentially. Briefly, after the first round of RNA FISH using a Cy3-labeled $(CAG)_{10}$ DNA probe, cells were subjected to prehybridization buffer (40% formamide, 2× SCC buffer, 200 μg/mL BSA, 100 mg/mL dextran sulfate, 2 mM vanadyl sulfate, and 1 mg/mL yeast tRNA [Invitrogen]) for 15 min at 37°C. The Alexa 488-labeled antisense oligo probe $(CTG)_{10}$ DNA was denatured for 10 min at 100°C, chilled on ice for 10 min, and then added to pre-chilled hybridization buffer to a final probe concentration of 500 pg/μL. The hybridization was performed in a humidified chamber for 2 hr at 37°C. After hybridization, cells were washed three times in pre-warmed 40% formamide and 2× SCC buffer for 30 min at 37°C and once in sterile PBS (pH 7.4), followed by counterstaining with Vectashield containing DAPI (Vector Laboratories). Cells were observed under an Olympus IX81-DSU Spinning Disk confocal microscope. The chamber was divided into 3 regions and 100 cells in each region were observed. The percentage of foci-negative cells among all the cells and antisense RNA CAG repeat foci among foci-negative cells were calculated and averaged.

Statistical Analysis

One-way ANOVA was used for statistical analyses and $p < 0.05$ was accepted as statistically significant.

SUPPLEMENTAL INFORMATION

Supplemental Information includes nine figures and one video and can be found with this article online at https://doi.org/10.1016/j.ymthe.2018.09.003.

AUTHOR CONTRIBUTIONS

Y.W. and L.H. contributed equally to the work; Y.W. contributed mainly to the targeted insertion of PolyA signals in 3′ UTR and L.H. contributed mainly to the targeted deletion of the CTG repeats. Study concept and design was contributed by G.X. Y.W., L.H., H.W., K.S., J.C., A.T., H.L., X.G., and G.X. acquired data. Analysis and interpretation of data were performed by G.X., Y.W., N.T., and T.A. G.X. and Y.W. drafted the manuscript with input from all the authors, particularly T.A. and N.T.

CONFLICTS OF INTEREST

The authors have no conflicts of interest.

ACKNOWLEDGMENTS

Research reported in this publication was supported by NIH/NIAMS grant K08 AR064836 to G.X., mentored by Maury S. Swanson, T.A., Laura Ranum, N.T., and S.H. Subramony at the University of Florida and Fernando Valenzuela at the University of New Mexico, and startup funds from the Office of Research at the Health Science Center of University of New Mexico. Special thanks to Jason Weick from the University of New Mexico who performed English language crafting and proofreading and Fernando Valenzuela from the University of New Mexico for critically reading the manuscript.

REFERENCES

1. Zhang, N., and Ashizawa, T. (2017). RNA toxicity and foci formation in microsatellite expansion diseases. Curr. Opin. Genet. Dev. *44*, 17–29.
2. Orr, H.T., and Zoghbi, H.Y. (2007). Trinucleotide repeat disorders. Annu. Rev. Neurosci. *30*, 575–621.
3. Maeder, M.L., and Gersbach, C.A. (2016). Genome-editing Technologies for Gene and Cell Therapy. Mol. Ther. *24*, 430–446.
4. Calos, M.P. (2017). Genome Editing Techniques and Their Therapeutic Applications. Clin. Pharmacol. Ther. *101*, 42–51.
5. Shim, G., Kim, D., Park, G.T., Jin, H., Suh, S.K., and Oh, Y.K. (2017). Therapeutic gene editing: delivery and regulatory perspectives. Acta Pharmacol. Sin. *38*, 738–753.
6. Cornu, T.I., Mussolino, C., and Cathomen, T. (2017). Refining strategies to translate genome editing to the clinic. Nat. Med. *23*, 415–423.
7. Mout, R., Ray, M., Lee, Y.W., Scaletti, F., and Rotello, V.M. (2017). In Vivo Delivery of CRISPR/Cas9 for Therapeutic Gene Editing: Progress and Challenges. Bioconjug. Chem. *28*, 880–884.
8. Schneller, J.L., Lee, C.M., Bao, G., and Venditti, C.P. (2017). Genome editing for inborn errors of metabolism: advancing towards the clinic. BMC Med. *15*, 43.
9. Mittelman, D., Moye, C., Morton, J., Sykoudis, K., Lin, Y., Carroll, D., and Wilson, J.H. (2009). Zinc-finger directed double-strand breaks within CAG repeat tracts promote repeat instability in human cells. Proc. Natl. Acad. Sci. USA *106*, 9607–9612.
10. van Agtmaal, E.L., André, L.M., Willemse, M., Cumming, S.A., van Kessel, I.D.G., van den Broek, W.J.A.A., Gourdon, G., Furling, D., Mouly, V., Monckton, D.G., et al. (2017). CRISPR/Cas9-Induced $(CTG{\cdot}CAG)_n$ Repeat Instability in the Myotonic Dystrophy Type 1 Locus: Implications for Therapeutic Genome Editing. Mol. Ther. *25*, 24–43.
11. Provenzano, C., Cappella, M., Valaperta, R., Cardani, R., Meola, G., Martelli, F., Cardinali, B., and Falcone, G. (2017). CRISPR/Cas9-Mediated Deletion of CTG Expansions Recovers Normal Phenotype in Myogenic Cells Derived from Myotonic Dystrophy 1 Patients. Mol. Ther. Nucleic Acids *9*, 337–348.
12. Fu, Y.H., Pizzuti, A., Fenwick, R.G., Jr., King, J., Rajnarayan, S., Dunne, P.W., Dubel, J., Nasser, G.A., Ashizawa, T., de Jong, P., et al. (1992). An unstable triplet repeat in a gene related to myotonic muscular dystrophy. Science *255*, 1256–1258.
13. Ashizawa, T., and Sarkar, P.S. (2011). Myotonic dystrophy types 1 and 2. Handb. Clin. Neurol. *101*, 193–237.
14. Romeo, V. (2012). Myotonic Dystrophy Type 1 or Steinert's disease. Adv. Exp. Med. Biol. *724*, 239–257.
15. Ranum, L.P., and Cooper, T.A. (2006). RNA-mediated neuromuscular disorders. Annu. Rev. Neurosci. *29*, 259–277.
16. Lee, J.E., and Cooper, T.A. (2009). Pathogenic mechanisms of myotonic dystrophy. Biochem. Soc. Trans. *37*, 1281–1286.
17. Gomes-Pereira, M., Cooper, T.A., and Gourdon, G. (2011). Myotonic dystrophy mouse models: towards rational therapy development. Trends Mol. Med. *17*, 506–517.
18. Park, C.Y., Kim, D.H., Son, J.S., Sung, J.J., Lee, J., Bae, S., Kim, J.H., Kim, D.W., and Kim, J.S. (2015). Functional Correction of Large Factor VIII Gene Chromosomal Inversions in Hemophilia A Patient-Derived iPSCs Using CRISPR-Cas9. Cell Stem Cell *17*, 213–220.

19. Gao, Y., Guo, X., Santostefano, K., Wang, Y., Reid, T., Zeng, D., Terada, N., Ashizawa, T., and Xia, G. (2016). Genome Therapy of Myotonic Dystrophy Type 1 iPS Cells for Development of Autologous Stem Cell Therapy. Mol. Ther. *24*, 1378–1387.

20. Xia, G., Gao, Y., Jin, S., Subramony, S.H., Terada, N., Ranum, L.P., Swanson, M.S., and Ashizawa, T. (2015). Genome modification leads to phenotype reversal in human myotonic dystrophy type 1 induced pluripotent stem cell-derived neural stem cells. Stem Cells *33*, 1829–1838.

21. Xia, G., Santostefano, K.E., Goodwin, M., Liu, J., Subramony, S.H., Swanson, M.S., Terada, N., and Ashizawa, T. (2013). Generation of neural cells from DM1 induced pluripotent stem cells as cellular model for the study of central nervous system neuropathogenesis. Cell. Reprogram. *15*, 166–177.

22. Xia, G., and Ashizawa, T. (2015). Dynamic changes of nuclear RNA foci in proliferating DM1 cells. Histochem. Cell Biol. *143*, 557–564.

23. Cong, L., Ran, F.A., Cox, D., Lin, S., Barretto, R., Habib, N., Hsu, P.D., Wu, X., Jiang, W., Marraffini, L.A., and Zhang, F. (2013). Multiplex genome engineering using CRISPR/Cas systems. Science *339*, 819–823.

24. Ran, F.A., Hsu, P.D., Lin, C.Y., Gootenberg, J.S., Konermann, S., Trevino, A.E., Scott, D.A., Inoue, A., Matoba, S., Zhang, Y., and Zhang, F. (2013). Double nicking by RNA-guided CRISPR Cas9 for enhanced genome editing specificity. Cell *154*, 1380–1389.

25. Cho, S.W., Kim, S., Kim, Y., Kweon, J., Kim, H.S., Bae, S., and Kim, J.S. (2014). Analysis of off-target effects of CRISPR/Cas-derived RNA-guided endonucleases and nickases. Genome Res. *24*, 132–141.

26. Jinek, M., Chylinski, K., Fonfara, I., Hauer, M., Doudna, J.A., and Charpentier, E. (2012). A programmable dual-RNA-guided DNA endonuclease in adaptive bacterial immunity. Science *337*, 816–821.

27. Davis, L., and Maizels, N. (2014). Homology-directed repair of DNA nicks via pathways distinct from canonical double-strand break repair. Proc. Natl. Acad. Sci. USA *111*, E924–E932.

28. Groenen, P.J., Wansink, D.G., Coerwinkel, M., van den Broek, W., Jansen, G., and Wieringa, B. (2000). Constitutive and regulated modes of splicing produce six major myotonic dystrophy protein kinase (DMPK) isoforms with distinct properties. Hum. Mol. Genet. *9*, 605–616.

29. Lam, L.T., Pham, Y.C., Nguyen, T.M., and Morris, G.E. (2000). Characterization of a monoclonal antibody panel shows that the myotonic dystrophy protein kinase, DMPK, is expressed almost exclusively in muscle and heart. Hum. Mol. Genet. *9*, 2167–2173.

30. Furling, D., Lemieux, D., Taneja, K., and Puymirat, J. (2001). Decreased levels of myotonic dystrophy protein kinase (DMPK) and delayed differentiation in human myotonic dystrophy myoblasts. Neuromuscul. Disord. *11*, 728–735.

31. Chal, J., Al Tanoury, Z., Hestin, M., Gobert, B., Aivio, S., Hick, A., Cherrier, T., Nesmith, A.P., Parker, K.K., and Pourquié, O. (2016). Generation of human muscle fibers and satellite-like cells from human pluripotent stem cells in vitro. Nat. Protoc. *11*, 1833–1850.

32. Li, J., Shou, J., Guo, Y., Tang, Y., Wu, Y., Jia, Z., Zhai, Y., Chen, Z., Xu, Q., and Wu, Q. (2015). Efficient inversions and duplications of mammalian regulatory DNA elements and gene clusters by CRISPR/Cas9. J. Mol. Cell Biol. *7*, 284–298.

33. Zu, T., Gibbens, B., Doty, N.S., Gomes-Pereira, M., Huguet, A., Stone, M.D., Margolis, J., Peterson, M., Markowski, T.W., Ingram, M.A., et al. (2011). Non-ATG-initiated translation directed by microsatellite expansions. Proc. Natl. Acad. Sci. USA *108*, 260–265.

34. Cleary, J.D., and Ranum, L.P. (2014). Repeat associated non-ATG (RAN) translation: new starts in microsatellite expansion disorders. Curr. Opin. Genet. Dev. *26*, 6–15.

35. Kearse, M.G., and Todd, P.K. (2014). Repeat-associated non-AUG translation and its impact in neurodegenerative disease. Neurotherapeutics *11*, 721–731.

36. Green, K.M., Linsalata, A.E., and Todd, P.K. (2016). RAN translation-What makes it run? Brain Res. *1647*, 30–42.

37. Ash, P.E., Bieniek, K.F., Gendron, T.F., Caulfield, T., Lin, W.L., Dejesus-Hernandez, M., van Blitterswijk, M.M., Jansen-West, K., Paul, J.W., 3rd, Rademakers, R., et al. (2013). Unconventional translation of C9ORF72 GGGGCC expansion generates insoluble polypeptides specific to c9FTD/ALS. Neuron *77*, 639–646.

38. Bañez-Coronel, M., Ayhan, F., Tarabochia, A.D., Zu, T., Perez, B.A., Tusi, S.K., Pletnikova, O., Borchelt, D.R., Ross, C.A., Margolis, R.L., et al. (2015). RAN Translation in Huntington Disease. Neuron *88*, 667–677.

39. Ishiguro, T., Sato, N., Ueyama, M., Fujikake, N., Sellier, C., Kanegami, A., Tokuda, E., Zamiri, B., Gall-Duncan, T., Mirceta, M., et al. (2017). Regulatory Role of RNA Chaperone TDP-43 for RNA Misfolding and Repeat-Associated Translation in SCA31. Neuron *94*, 108–124.e7.

40. Krans, A., Kearse, M.G., and Todd, P.K. (2016). Repeat-associated non-AUG translation from antisense CCG repeats in fragile X tremor/ataxia syndrome. Ann. Neurol. *80*, 871–881.

41. Mori, K., Weng, S.M., Arzberger, T., May, S., Rentzsch, K., Kremmer, E., Schmid, B., Kretzschmar, H.A., Cruts, M., Van Broeckhoven, C., et al. (2013). The C9orf72 GGGGCC repeat is translated into aggregating dipeptide-repeat proteins in FTLD/ALS. Science *339*, 1335–1338.

42. Todd, P.K., Oh, S.Y., Krans, A., He, F., Sellier, C., Frazer, M., Renoux, A.J., Chen, K.C., Scaglione, K.M., Basrur, V., et al. (2013). CGG repeat-associated translation mediates neurodegeneration in fragile X tremor ataxia syndrome. Neuron *78*, 440–455.

43. Zu, T., Liu, Y., Bañez-Coronel, M., Reid, T., Pletnikova, O., Lewis, J., Miller, T.M., Harms, M.B., Falchook, A.E., Subramony, S.H., et al. (2013). RAN proteins and RNA foci from antisense transcripts in C9ORF72 ALS and frontotemporal dementia. Proc. Natl. Acad. Sci. USA *110*, E4968–E4977.

44. Zu, T., Cleary, J.D., Liu, Y., Bañez-Coronel, M., Bubenik, J.L., Ayhan, F., Ashizawa, T., Xia, G., Clark, H.B., Yachnis, A.T., Swanson, M.S., and Ranum, L.P.W. (2017). RAN Translation Regulated by Muscleblind Proteins in Myotonic Dystrophy Type 2. Neuron *95*, 1292–1305.e5.

45. Jansen, G., Groenen, P.J., Bächner, D., Jap, P.H., Coerwinkel, M., Oerlemans, F., van den Broek, W., Gohlsch, B., Pette, D., Plomp, J.J., et al. (1996). Abnormal myotonic dystrophy protein kinase levels produce only mild myopathy in mice. Nat. Genet. *13*, 316–324.

46. Berul, C.I., Maguire, C.T., Aronovitz, M.J., Greenwood, J., Miller, C., Gehrmann, J., Housman, D., Mendelsohn, M.E., and Reddy, S. (1999). DMPK dosage alterations result in atrioventricular conduction abnormalities in a mouse myotonic dystrophy model. J. Clin. Invest. *103*, R1–R7.

47. Lee, H.C., Patel, M.K., Mistry, D.J., Wang, Q., Reddy, S., Moorman, J.R., and Mounsey, J.P. (2003). Abnormal Na channel gating in murine cardiac myocytes deficient in myotonic dystrophy protein kinase. Physiol. Genomics *12*, 147–157.

48. Pall, G.S., Johnson, K.J., and Smith, G.L. (2003). Abnormal contractile activity and calcium cycling in cardiac myocytes isolated from DMPK knockout mice. Physiol. Genomics *13*, 139–146.

49. Reddy, S., Smith, D.B., Rich, M.M., Leferovich, J.M., Reilly, P., Davis, B.M., Tran, K., Rayburn, H., Bronson, R., Cros, D., et al. (1996). Mice lacking the myotonic dystrophy protein kinase develop a late onset progressive myopathy. Nat. Genet. *13*, 325–335.

50. Kosicki, M., Tomberg, K., and Bradley, A. (2018). Repair of double-strand breaks induced by CRISPR-Cas9 leads to large deletions and complex rearrangements. Nat. Biotechnol. *36*, 765–771.

51. Law, P.K., Bertorini, T.E., Goodwin, T.G., Chen, M., Fang, Q.W., Li, H.J., Kirby, D.S., Florendo, J.A., Herrod, H.G., and Golden, G.S. (1990). Dystrophin production induced by myoblast transfer therapy in Duchenne muscular dystrophy. Lancet *336*, 114–115.

52. Gussoni, E., Pavlath, G.K., Lanctot, A.M., Sharma, K.R., Miller, R.G., Steinman, L., and Blau, H.M. (1992). Normal dystrophin transcripts detected in Duchenne muscular dystrophy patients after myoblast transplantation. Nature *356*, 435–438.

53. Huard, J., Bouchard, J.P., Roy, R., Malouin, F., Dansereau, G., Labrecque, C., Albert, N., Richards, C.L., Lemieux, B., and Tremblay, J.P. (1992). Human myoblast transplantation: preliminary results of 4 cases. Muscle Nerve *15*, 550–560.

54. Mendell, J.R., Kissel, J.T., Amato, A.A., King, W., Signore, L., Prior, T.W., Sahenk, Z., Benson, S., McAndrew, P.E., Rice, R., et al. (1995). Myoblast transfer in the treatment of Duchenne's muscular dystrophy. N. Engl. J. Med. *333*, 832–838.

55. Morandi, L., Bernasconi, P., Gebbia, M., Mora, M., Crosti, F., Mantegazza, R., and Cornelio, F. (1995). Lack of mRNA and dystrophin expression in DMD patients three months after myoblast transfer. Neuromuscul. Disord. *5*, 291–295.

56. Karpati, G., Ajdukovic, D., Arnold, D., Gledhill, R.B., Guttmann, R., Holland, P., Koch, P.A., Shoubridge, E., Spence, D., Vanasse, M., et al. (1993). Myoblast transfer in Duchenne muscular dystrophy. Ann. Neurol. *34*, 8–17.

57. Bajek, A., Porowinska, D., Kloskowski, T., Brzoska, E., Ciemerych, M.A., and Drewa, T. (2015). Cell therapy in Duchenne muscular dystrophy treatment: clinical trials overview. Crit. Rev. Eukaryot. Gene Expr. *25*, 1–11.

58. Montarras, D., Morgan, J., Collins, C., Relaix, F., Zaffran, S., Cumano, A., Partridge, T., and Buckingham, M. (2005). Direct isolation of satellite cells for skeletal muscle regeneration. Science *309*, 2064–2067.

59. Gilbert, P.M., Havenstrite, K.L., Magnusson, K.E., Sacco, A., Leonardi, N.A., Kraft, P., Nguyen, N.K., Thrun, S., Lutolf, M.P., and Blau, H.M. (2010). Substrate elasticity regulates skeletal muscle stem cell self-renewal in culture. Science *329*, 1078–1081.

60. Takahashi, K., Tanabe, K., Ohnuki, M., Narita, M., Ichisaka, T., Tomoda, K., and Yamanaka, S. (2007). Induction of pluripotent stem cells from adult human fibroblasts by defined factors. Cell *131*, 861–872.

61. Yu, J., Vodyanik, M.A., Smuga-Otto, K., Antosiewicz-Bourget, J., Frane, J.L., Tian, S., Nie, J., Jonsdottir, G.A., Ruotti, V., Stewart, R., et al. (2007). Induced pluripotent stem cell lines derived from human somatic cells. Science *318*, 1917–1920.

62. Meissner, A., Wernig, M., and Jaenisch, R. (2007). Direct reprogramming of genetically unmodified fibroblasts into pluripotent stem cells. Nat. Biotechnol. *25*, 1177–1181.

63. Gudde, A.E.E.G., van Heeringen, S.J., de Oude, A.I., van Kessel, I.D.G., Estabrook, J., Wang, E.T., Wieringa, B., and Wansink, D.G. (2017). Antisense transcription of the myotonic dystrophy locus yields low-abundant RNAs with and without (CAG)n repeat. RNA Biol. *14*, 1374–1388.

64. Klesert, T.R., Otten, A.D., Bird, T.D., and Tapscott, S.J. (1997). Trinucleotide repeat expansion at the myotonic dystrophy locus reduces expression of DMAHP. Nat. Genet. *16*, 402–406.

65. Thornton, C.A., Wymer, J.P., Simmons, Z., McClain, C., and Moxley, R.T., 3rd (1997). Expansion of the myotonic dystrophy CTG repeat reduces expression of the flanking DMAHP gene. Nat. Genet. *16*, 407–409.

66. Inukai, A., Doyu, M., Kato, T., Liang, Y., Kuru, S., Yamamoto, M., Kobayashi, Y., and Sobue, G. (2000). Reduced expression of DMAHP/SIX5 gene in myotonic dystrophy muscle. Muscle Nerve *23*, 1421–1426.

67. Brouwer, J.R., Huguet, A., Nicole, A., Munnich, A., and Gourdon, G. (2013). Transcriptionally Repressive Chromatin Remodelling and CpG Methylation in the Presence of Expanded CTG-Repeats at the DM1 Locus. J. Nucleic Acids *2013*, 567435.

68. Klesert, T.R., Cho, D.H., Clark, J.I., Maylie, J., Adelman, J., Snider, L., Yuen, E.C., Soriano, P., and Tapscott, S.J. (2000). Mice deficient in Six5 develop cataracts: implications for myotonic dystrophy. Nat. Genet. *25*, 105–109.

69. Sarkar, P.S., Appukuttan, B., Han, J., Ito, Y., Ai, C., Tsai, W., Chai, Y., Stout, J.T., and Reddy, S. (2000). Heterozygous loss of Six5 in mice is sufficient to cause ocular cataracts. Nat. Genet. *25*, 110–114.

70. Mankodi, A., Logigian, E., Callahan, L., McClain, C., White, R., Henderson, D., Krym, M., and Thornton, C.A. (2000). Myotonic dystrophy in transgenic mice expressing an expanded CUG repeat. Science *289*, 1769–1773.

71. Seznec, H., Agbulut, O., Sergeant, N., Savouret, C., Ghestem, A., Tabti, N., Willer, J.C., Ourth, L., Duros, C., Brisson, E., et al. (2001). Mice transgenic for the human myotonic dystrophy region with expanded CTG repeats display muscular and brain abnormalities. Hum. Mol. Genet. *10*, 2717–2726.

72. Stemmer, M., Thumberger, T., Del Sol Keyer, M., Wittbrodt, J., and Mateo, J.L. (2015). CCTop: An Intuitive, Flexible and Reliable CRISPR/Cas9 Target Prediction Tool. PLoS ONE *10*, e0124633.

73. Akiyama, T., Wakabayashi, S., Soma, A., Sato, S., Nakatake, Y., Oda, M., Murakami, M., Sakota, M., Chikazawa-Nohtomi, N., Ko, S.B., and Ko, M.S. (2016). Transient ectopic expression of the histone demethylase JMJD3 accelerates the differentiation of human pluripotent stem cells. Development *143*, 3674–3685.

74. Liu, Y., Pattamatta, A., Zu, T., Reid, T., Bardhi, O., Borchelt, D.R., Yachnis, A.T., and Ranum, L.P. (2016). C9orf72 BAC Mouse Model with Motor Deficits and Neurodegenerative Features of ALS/FTD. Neuron *90*, 521–534.